HHS Public Access

Author manuscript

Mol Imaging Biol. Author manuscript; available in PMC 2018 October 01.

Published in final edited form as:

Mol Imaging Biol. 2017 October ; 19(5): 703–713. doi:10.1007/s11307-016-1038-6.

A Novel Modality for Functional Imaging in Acute Intervertebral Disk Herniation via Tracking Leukocyte Infiltration

Li Xiao[1], **Mengmeng Ding**[1], **Yi Zhang**[2,3], **Mahendra Chordia**[2], **Dongfeng Pan**[2], **Adam Shimer**[1], **Francis Shen**[1], **David Glover**[4], **Li Jin**[1], and **Xudong Li**[1]

[1]Department of Orthopaedic Surgery, University of Virginia, Rm B051, Cobb Hall, 135 Hospital Dr., Charlottesville, VA, 22908, USA

[2]Department of Radiology and Biomedical Imaging, University of Virginia, Charlottesville, VA, 22908, USA

[4]Department of Cardiovascular Medicine, University of Virginia, Charlottesville, 22908, USA

Abstract

Purpose—Inflammation plays a key role in the progression of intervertebral disk (IVD) herniation and associated low back pain. However, real-time spatial diagnosis of inflammation associated with acute disk herniation has not been investigated. We sought to detect local neutrophil and macrophage infiltration near disk herniation via the formyl peptide receptor 1 (FPR1)-mediated molecular imaging in a disk puncture mouse model to elucidate pathophysiological process of disk herniation.

Procedures—Disk herniation was induced in mouse with an established needle puncture procedure. Degenerative change of disk and infiltration of neutrophils and macrophages were detected with Safranin-O, hematoxylin and eosin (H&E), and immunohistochemical staining after injury. FPR1-specific imaging probes cFLFLF-PEG-Cy7 and [^{99m}Tc]HYNIC-PEG-cFLFLF were administered systemically to sham and disk injury mice. Leukocyte infiltration was tracked by *in vivo* near-infrared fluorescence (NIRF) and single-photon emission tomography (SPECT) imaging. The peptide-receptor binding specificity was further investigated with FPR1$^{-/-}$ mice via *ex vivo* NIRF scan and *in vitro* binding assays.

Results—Safranin-O staining exhibited disorganized disk structure and loss of proteoglycan after puncture. Massive inflammatory cells were observed in the anterior region of punctured annulus in the injury group. The majority of neutrophils were detected at 1 through 3 days, while infiltration of macrophages appeared the most at 7 days after injury. NIRF and SPECT images revealed preferential accumulation of cFLFLF probes in herniation site in wild-type mice but not in FPR1$^{-/-}$ mice. Binding of the cFLFLF peptide to FPR1 was also observed in RAW 267.4 cells and

Correspondence to: Xudong Li; lispine@icloud.com.

[3]Present address: Biomedical Imaging Research Institute, Cedars-Sinai Medical Center, 8700 Beverly Blvd. Davis Building, Rm G140, Los Angeles, CA, 90048, USA

Compliance with Ethical Standards

Conflict of Interest

The authors declare that they have no conflict of interest.

Electronic supplementary material The online version of this article (doi:10.1007/s11307-016-1038-6) contains supplementary material, which is available to authorized users.

macrophages isolated from wild-type mice, whereas much less signal was observed in macrophages from FPR1$^{-/-}$ mice. The presence of macrophage infiltration was also detected in human-herniated disk samples by immunohistochemistry.

Conclusion—For the first time, leukocyte infiltration around acute disk herniation site was detected directly and non-invasively in a timely fashion using FPR1-targeted molecular imaging modalities. Such functional imaging of disk herniation via infiltrated leukocytes would advance the understanding of etiology and facilitate drug delivery and treatment monitoring of disk herniation.

Keywords

Low back pain; Acute disk herniation; Leukocyte infiltration; Formyl peptide receptor (FPR) 1; Near-infrared fluorescence imaging (NIRF); Single-photon emission computed tomography (SPECT); Neutrophil; Macrophage

Introduction

Low back pain with or without radiculopathy is a leading source of disability with national economic losses of over $100 billion per year [1]. Intervertebral disk (IVD) degeneration is one of the predominant causes of low back pain with lifetime prevalence of 70 to 85 % [2]. Despite considerable research efforts, the etiology of disk degeneration remains unclear and current treatments of low back pain still rely upon symptom relief [3].

Inflammation is a key player in the progression of radiculopathy [4]. Following herniation, nucleus pulposus (NP) pinches the nerves causing inflammation by chemical irritation or as secondary reactions to an autoimmune response against NP from surrounding tissues [4]. Immunological response may be triggered by activation and recruitment of leukocytes to exaggerate the pro-inflammatory feedback loop [4]. In addition, both disk cells and infiltrated immune cells produce pro-inflammatory mediators such as cytokines, further exacerbating the inflammatory response [5]. Given this, non-invasive detection of this inflammatory process would be a significant breakthrough for early diagnosis and pathological understanding of radiculopathy.

Over the last few decades, molecular imaging has undergone tremendous development in drug discovery and characterization of pathological process. Herein, we hypothesize that infiltrated leukocytes around herniated disk can be a good target for functional and molecular imaging to detect and monitor immunological responses of acute disk herniation. Formyl peptide receptor 1 (FPR1) is a cornerstone of cell chemotaxis and activation and is highly expressed on activated neutrophils and monocytes/macrophages in the inflammatory processes [6]. We sought to target FPR1 expressed on infiltrated leukocytes upon acute disk herniation with a known antagonistic peptidomimetic cinnamoyl-D-leucyl-phenylalanyl-D-leucyl-phenylalanyl-leucyl-phenylalanine (cFLFLF) by molecular imaging (Supplemental Fig. 1). *In vivo* near-infrared fluorescence (NIRF) and single-photon emission tomography (SPECT) imaging were performed in wild-type (WT) mice after disk puncture. Timing and response of neutrophil and macrophage infiltration were deciphered in a disk herniation mouse model. In addition, FPR1 knockout (FPR1$^{-/-}$) mouse strain was adopted to validate

receptor-mediated probe binding. Our results presented a new functional and molecular imaging modality for acute disk herniation. Success of the project would ultimately benefit early diagnosis, pathophysiological understanding, and drug discovery of disk herniation.

Materials and Methods

Chemicals and Reagents

Fmoc-PAL-PEG-PS resin was procured from Applied Biosystems (Foster City, CA). *t*-Boc-PEG-NHS 3.4 kD was obtained from Laysan Bio Inc. (Arab, AL). Cy7 Mono NHS ester was purchased from GE Healthcare Life Sciences (Piscataway, NJ). High-performance liquid chromatography (HPLC) grade solvents were purchased from Fisher Scientific (Pittsburgh, PA). Na[^{99m}Tc]TcO_4 was obtained from Cardinal Health, Inc. (Charlottesville, VA). 6-Boc-hydrazinonicotinic acid (6-Boc-HYNIC acid) was obtained from SoluLink (San Diego, CA). Gibco Dulbecco's modified Eagle medium (high glucose 4.5 g/l) (DMEM), fetal bovine serum (FBS), penicillin/streptomycin (Pen/Strep), and Prolong Gold antifade reagent with 4′,6-diamidino-2-phenylindole (DAPI) were purchased from Life Technologies (Grand Island, NY). Other chemicals were obtained from Sigma-Aldrich (St. Louis, MO) unless mentioned.

Synthesis of NIRF and SPECT Imaging Probes

NIRF (cFLFLF-PEG-Cy7) and SPECT ([^{99m}Tc]HYNIC-PEG-cFLFLF) imaging probes were synthesized and characterized following published procedures (Supplemental Materials for details) [7–9].

Mouse Model of Disk Herniation

Animal procedures and *in vivo* studies were approved by the Institutional Animal Care and Use Committee (IACUC). Disk needle puncture and sham surgeries were performed in WT (Balb-c, female, 8–12 weeks, Jackson Laboratory) and FPR1$^{-/-}$ mice (female, 8–12 weeks, Taconic Bioscience) according to published protocols [10]. Using aseptic techniques, the spine was exposed through an anterior midline transperitoneal approach after animal anesthesia. L3–4 and L4–5 disks were punctured with a 27-gauge needle (Hamilton, Reno, NV). For the sham group, L3–4 and L4–5 disks were exposed without needle puncture. A total of 38 WT mice were employed for NIRF (n = 30) and SPECT (n = 8) imaging, randomly assigning half of them as disk puncture (injury) group and another half as mock surgery (sham) group. FPR1$^{-/-}$ mice (n = 12) were used for NIRF imaging and *in vitro* binding studies. Based on our previous data, for the outcomes of *ex vivo* NIRF quantification with a standard deviation of 20 %, a power of 0.85 would be achieved with a sample size of 5 for each group to detect a mean difference of 50 % in the NIRF imaging experiments.

SPECT Imaging

Seven days after surgery, SPECT probe [^{99m}Tc]HYNIC-PEG-cFLFLF (~1–2 mCi) was intravenously injected into injury (n = 4) and sham WT mice (n = 4). At about 2–3 h post injection, SPECT imaging was performed using a Siemens Orbiter camera outfit with a customized 1.5-mm tungsten pinhole collimator. Images were collected in a 128 × 128 count

matrix with 64 frames at 30 s/frame and reconstructed using an OSEM algorithm (ReSPECT, Bioscan Inc., Washington DC).

Near-Infrared Fluorescence Imaging

Three hours after disk surgery, probe cFLFLF-PEG-Cy7 (2 nmol per 20 g mouse) was administered via tail veins. At various time points post probe injection (pi), *in vivo* and *ex vivo* imaging were acquired [11]. Mice were then euthanized, and lumbar spines were harvested for *ex vivo* imaging. For FPR1$^{-/-}$ mice, transillumination fluorescence imaging was not achievable due to the black fur of this mouse strain. However, this difficulty was overcome with *ex vivo* imaging of lumbar tissue from both injury and sham groups of FPR1$^{-/-}$ mice at 3 days post injection by comparing with the corresponding WT mice groups.

Immunofluorescence Staining of WT and FPR1$^{-/-}$ Macrophages

Macrophage isolation from mouse intraperitoneal cavity was performed [12]. Isolated peritoneal macrophages from WT and FPR1$^{-/-}$ mice were cultured on a 4-well chamber (Thermo Fisher Scientific, Waltham, MA) at a density of 1×10^5 cells per chamber at 37 °C overnight. Cells were fixed with 4 % paraformaldehyde for 30 min, permeabilized with 0.3 % Triton X-100 for 5 min, and blocked with 3 % bovine serum albumin in PBS for 1 h. Cells were incubated with cFLFLF-PEG-Cy3 (1 μM) for 30 min, washed and stained with biotinylated anti-mouse MAC-2 mAb (1:500, Cedarlane, Burlington, NC) for 2 h, and followed by FITC-conjugated streptavidin (1:1000, eBioscience, San Diego, CA) incubation for 30 min. Cell nuclei were counterstained with DAPI. Negative control was performed with identical procedures excluding incubation with primary antibody. Fluorescence images were taken with a confocal fluorescence microscope (LSM 510-UV, Carl Zeiss, Germany) and processed by LSM Image Browser software (Carl Zeiss, Germany).

Fluorescence-Activated Cell Sorting

Homogeneous suspensions of RAW 264.7 and intraperitoneally harvested macrophages (WT or FPR1$^{-/-}$) were prepared in PBS at a density of 1×10^6 cells/ml (200 μl/sample) and incubated with fluorescent peptide cFLFLF-PEG-Cy7 (Cy3) (1 μM in PBS) for 30 min at 37 °C. Following incubation, cells were washed with PBS to remove non-bound peptide and fixed with 2 % paraformaldehyde at 4 °C overnight. Suspension was passed through a nylon mesh of 100-μm pore size before fluorescence-activated cell sorting (FACS) assay. Cell suspension in control groups was prepared with identical procedures excluding peptide incubation. At least 10,000 events were counted on a FACS Calibur Benchtop Analyzer (BD Biosciences, San Jose, CA) with the machine gated for live cells based on forward scatter and side scatter. Percentages of cells bound with the peptide were determined out of the total 10,000 events by detecting Cy3 (580-nm bandwidth filter) or Cy7 (740-nm long path filter) fluorescence intensities. Data were analyzed and displayed as dot plots using FlowJo software (TreeStar, Ashland, OR).

In Vitro FPR1-Targeted cFLFLF-PEG-Cy7 Binding to Macrophages

In a black clear BD Falcon 96-well plate (BD Biosciences, San Jose, CA), RAW 264.7, WT, and FPR1$^{-/-}$ macrophages were suspended in complete growth medium (DMEM + 10 % FBS + 1 % penicillin/streptomycin) at a density of 4×10^4 cells per well and incubated overnight at 37 °C. Cells were incubated with three concentrations of imaging agent cFLFLF-PEG-Cy7 (10, 1, and 0.1 μM) in serum-free DMEM for 30 min at 37 °C and washed with PBS with 100 μl PBS remaining in each well. The plate was scanned with LI-COR Odyssey Infrared Imaging System (LI-COR Biotechnology, Lincoln, NE). Cells were lysed in 0.1 % SDS for total protein assay with Bio-Rad D_C protein assay reagents (Bio-Rad Laboratories, Hercules, CA). The fluorescence intensity was normalized to total protein content and presented as a mean of triplicates.

Safranin-O and Hematoxylin/Eosin Staining

Lumbar spinal columns were fixed in 10 % formalin, decalcified with 0.25 M ethylenediaminetetraacetic acid (EDTA), embedded in paraffin, sectioned midsagittally (5 μm), and stained with 0.1 % Safranin-O (counterstained by fast green) to detect structural change and proteoglycan content or hematoxylin and eosin (H&E) for identification of cell infiltration and disk structural change [10].

Immunohistochemical Detection and Quantification of Neutrophils and Macrophages

Immunohistochemistry was performed to detect infiltrated neutrophils and macrophages in mouse disk [13]. In brief, endogenous hydroperoxidase was blocked with 2 % H_2O_2/methanol for 30 min, followed by antigen retrieval in sodium citrate buffer (10 mM, pH 6.0) at 85 °C for 30 min, and non-specific signal blocking for 1 h. Sections were incubated with either rat antineutrophil monoclonal antibody (1:100, Thermo Scientific) or biotinylated anti-mouse MAC-2 mAb (1:200) at 4 °C overnight. For neutrophil detection, biotinylated goat-anti-rat secondary antibody (1:200) (Vector Laboratories Inc., Burlingame, CA) was used. The signal was visualized with 3,3′-diaminobenzidine (DAB). Hematoxylin was used for counterstaining. IgG control was performed following identical procedures excluding the primary antibody incubation.

Microscopic images of immunostained lumbar sections (injury and sham) were taken by Nikon ECLIPSE E600 with Zeiss software. At a magnification of ×400 for each injured disk with tissue area of 0.16 mm^2 and volume of 0.79×10^{-3} mm^3, three distinct field of views were randomly selected from anterior edges adjacent to punctured annulus. The number of infiltrated neutrophils and macrophages per unit area was counted. Two injured disks were assessed per lumbar section. Three sections centered on the needle puncture trajectory were analyzed per mouse. Five mice were analyzed per time point per group.

Immunostaining of Human Soft Tissue Adjacent to Herniated Disk

Following approved guidelines set by the US National Institutes of Health Office of Human Subjects Research for use of surgical waste and approved by Institutional Review Board for Health Science Research, soft tissues surrounding degenerated disks were obtained from five patients who had undergone microdiscectomy. These samples were processed as above for H&E and immunostaining.

Statistical Analysis

All data were presented as mean ± standard deviation (SD). Statistical analysis for cell binding assays and *ex vivo* imaging was performed by one-way ANOVA and corrected by Tukey's post hoc tests using Origin Software. Any p value less than 0.05 was considered statistically significant.

Results

Degenerative Change and Inflammatory Cell Infiltration Following Disk Puncture

Safranin-O staining was performed to confirm degenerative change in disk upon needle puncture. Meanwhile, H&E staining was performed to further identity the infiltration of inflammatory cells. As shown in Fig. 1a, Safranin-O staining exhibited loss of NP, disoriented annulus fibrosus (AF), and decreased proteoglycan (lessened red color) in injured disks as early as 1 day post injury compared to the sham, confirming degenerative change in injured disks (Fig. 1a). Massive cell infiltration was observed in tissue adjacent to anterior AF, in particular, at 7 days after injury via both Safranin-O (Fig. 1a) and H&E staining (Fig. 1b). There was a distinguishable change in color of injured disks appeared at 7 days post injury, compared with intact disks (Supplemental Fig. 2). Similar inflammatory cell infiltration was also observed in FPR1$^{-/-}$ mice after 3 days of disk injury (Supplemental Fig. 3).

Neutrophil and Macrophage Infiltration in Herniated IVDs

Neutrophils (brown cells as indicated by arrows) appeared as early as 1 day, remained visible until 3 days, and almost disappeared at 7 days post injury in regions adjacent to anterior AF (Fig. 2a) in injury group. A few neutrophils were also observed in the sham group (Fig. 2b). On the other hand, infiltration of macrophages exhibited a distinct pattern (Fig. 2c). Macrophages were not detected at 1 day, slightly increased at 3 days, and massively infiltrated at 7 days (arrows); in contrast, very few macrophages were observed in the sham group at any given time point up to 7 days post injury (Fig. 2d). Figure 2e illustrates quantification of immunopositive cells. The number of neutrophils infiltrated per unit tissue volume (0.79×10^{-3} mm^3) was 17.0 ± 3.2 cells at 1 day, 7.5 ± 1.9 cells at 3 days, and none at 7 days post injury. In contrast, the number of macrophages infiltrated per unit tissue volume (0.79×10^{-3} mm^3) appeared as 3.6 ± 1.2 cells at 1 day, 21.3 ± 2.9 cells at 3 days, and 58.4 ± 9.0 at 7 days post injury. In corroboration, the presence of macrophage infiltration was also detected in the tissue of herniated disk from patients (Fig. 2f).

Non-invasive SPECT Imaging of Injured IVD

The precursor cFLFLF-PEG-HYNIC was radiolabeled with Tc-99m with >95 % purity (Supplemental Fig. 4). In our prior study, SPECT probe showed good neutrophil-binding affinity (K_d = 15.48 nM) and minimal agonist activity at all concentrations. The specific activity of the purified [^{99m}Tc]cFLFLF was assessed to be 12.2 GBq/μmol [7, 9]. SPECT imaging revealed highly specific accumulation of radioactive signal in disk herniation site in proximity to kidneys (Fig. 3a), while no focal signal was observed in the corresponding disk

region of sham (Fig. 3b) at 7 days post injury, suggesting site-specific targeting and accumulation of cFLFLF peptide in herniated disks.

In Vivo NIRF Imaging Detected Herniated Intervertebral Disk

Longitudinal transillumination (3D view) NIRF imaging exhibited a strong signal in the region closely associated with herniated disks up to 7 days after injury (Fig. 4a) (yellow arrows), whereas no visible signal was observed in the equivalent region of sham (Fig. 4b). Fluorescence intensity at disk of interest in injured mice dropped by 49 % from 4 to 24 h and remained as a plateau up to 7 days (Fig. 4c).

Ex Vivo Lumbar Fluorescence Imaging Confirmed Target-Specific and FPR1-Mediated Spatial Distribution of Probe cFLFLF-PEG-Cy7 in Herniated Disks

Fluorescence signal was clearly discernible in injured disk sites at all three time points in WT mice (Fig. 5a). In contrast, the sham group demonstrated minimal baseline signal compared with the injury group under the same intensity scale. Figure 5b reveals major probe retention in liver and kidneys up to 7 days pi, whereas fluorescence signal was barely detectable in other organs. Disk fluorescence signal intensities in average radiant efficiency ([p/s/cm^2/sr]/[μW/cm^2]) in WT injured and sham groups were $7.82 \times 10^6 \pm 1.25 \times 10^6$ and $2.44 \times 10^6 \pm 1.52 \times 10^6$, respectively, at 1 day (**$p = 0.0027$), $4.75 \times 10^6 \pm 1.47 \times 10^6$ and $2.08 \times 10^6 \pm 1.33 \times 10^6$, respectively, at 3 days (*$p = 0.0084$) and $5.31 \times 10^6 \pm 1.05 \times 10^6$ and $2.09 \times 10^6 \pm 0.55 \times 10^6$, respectively, at 7 days (**$p = 0.0027$) (Fig. 5c). Significantly higher probe accumulation in injured disks compared to sham disks was consistently observed at all three time points, suggesting superior and long-lasting NIRF signal due to the presence of peptide bound with infiltrated leukocytes expressing FPR1 in herniated disk. However, at 3 days post surgery, *ex vivo* fluorescence intensity in average radiant efficiency ([p/s/cm^2/sr]/[μW/cm^2]) in injury/WT ($4.75 \times 10^6 \pm 1.47 \times 10^6$) showed much stronger signal than the other three groups (*$p = 0.0084$ vs. WT/sham, *$p = 0.0035$ vs. sham/FPR$^{-/-}$, *$p = 0.0029$ vs. injury/FPR$^{-/-}$) and the fluorescence signal in the latter three groups revealed no significant difference [for injury/FPR1$^{-/-}$, $1.88 \times 10^6 \pm 0.30 \times 10^6$; for sham/FPR1$^{-/-}$, $1.93 \times 10^6 \pm 0.38 \times 10^6$; for sham/WT, $2.08 \times 10^6 \pm 1.33 \times 10^6$] ($p = 0.85$ for injury/FPR1$^{-/-}$ vs. sham/FPR1$^{-/-}$ and $p = 0.75$ for injury/FPR1$^{-/-}$ vs. sham/WT) (Fig. 5d, e). In addition, *ex vivo* probe-tissue binding showed stronger and more localized fluorescence signal in the anterior side of injury disk (7 days) compared to sham (Supplemental Fig. 6). These results confirmed that observed NIRF signal in injured disk of WT was mainly contributed by FPR1-mediated cFLFLF probe binding and the presence of leukocytes in inflamed sites.

In Vitro FPR1-Mediated Probe Binding with Macrophage

Both WT and FPR1$^{-/-}$ macrophages were stained positively (green) for MAC2. WT macrophages showed positive peptide binding (red), whereas FPR1$^{-/-}$ macrophages exhibited little binding, suggesting peptide binds with macrophages via FPR1 (Fig. 6a). Similarly, RAW 264.7 (established cell line as positive control) and WT macrophages showed more than 90 % of cell binding with the fluorescent peptide, whereas FPR1$^{-/-}$ cells revealed much less binding using FACS (Fig. 6b). A cell binding assay in 96-well plate also demonstrated visually stronger fluorescence (indicative of greater peptide binding) for RAW

264.7 and WT macrophages than that of FPR1$^{-/-}$ cells (Fig. 6c). Figure 6d shows quantified results of preferential binding of the probe towards RAW 264.7 and WT macrophages compared to FPR1$^{-/-}$ macrophages (*p = 0.008 for FPR1$^{-/-}$ macrophages vs. RAW cells, **p = 0.002 for FPR1$^{-/-}$ vs. WT macrophages).

Discussion

Recent findings have uncovered the role of inflammation in disk herniation and discogenic low back pain [4, 14]. In particular, leukocytes (neutrophils, macrophages, and T and B lymphocytes) have been observed in degenerative disk in animals and human [15, 16]. In our study, we observed macrophage infiltration in human disk herniation sites (Fig. 2f), consistent with literature reports that approximately 36–66 % of surgically obtained human-herniated disk specimens expressed abundant macrophage infiltration, as a prominent source of inflammation and pain [17–19]. The evidence suggests that inflammatory leukocytes play a critical role in the progression of disk herniation and back pain. However, the response episodes of inflammatory leukocytes and their correlation to progression of disk herniation have not been completely deciphered in literatures. Our new imaging approach will provide invaluable information to deepen our understanding.

In the present study, we induced the mouse lumbar disk herniation via needle puncture and confirmed the degenerative change by well-established Safranin-O and H&E staining as shown in Fig. 1. The time-dependent infiltration of inflammatory leukocytes upon injury was then validated with immuno-histochemical staining as demonstrated in Fig. 2. From these observations, it was evident that neutrophils and macrophages were recruited into the disk herniation site sequentially over time post injury (from 1 through 7 days) with an early neutrophil phase followed by macrophages in the later phase in the injury group, while neither neutrophil nor macrophage was observed in the sham mice (Fig. 2a–e). One possible reason of fluorescence intensity remaining as a high plateau in injured disks up to 7 days after a single probe injection (Figs. 4 and 5) might be contributed by neutrophil infiltration primarily at 1 day, a combination of neutrophils and macrophages at 3 days, and mainly macrophages at 7 days. Although our approach might not be able to distinguish neutrophils and macrophages at a given time point in this acute disk herniation model, it proved feasibility to detect cell and event-specific leukocyte infiltration would benefit piece together the orchestrated inflammatory process in acute disk herniation.

The FPR specificity of cFLFLF-based probes has been examined by receptor blocking studies and scrambled peptide in previous efforts [11, 20]. FPR1$^{-/-}$ mice developed normally with impaired antibacterial host defense when challenged with bacterial [21]. Using FPR1$^{-/-}$ mice, we addressed FPR1-mediated binding specificity at a molecular level (Fig. 5). *Ex vivo* imaging suggested that the predominant signal accumulation was resulted from FPR1 targeting and minimum background signal might emit from other isoforms of FPRs (Fig. 5d). Accordingly, preferential *in vitro* binding of cFLFLF peptide to FPR1 receptor was confirmed in WT and RAW macrophages when compared with macrophages isolated from FPR1$^{-/-}$ mice (Fig. 6). These observations provided direct evidence regarding the targeting and preferential binding of cFLFLF peptide. To the best of our knowledge, this

is the first study employing FPR1$^{-/-}$ mouse strain in imaging inflammatory process and disk research.

There are some limitations in this study. First of all, mouse disk puncture model may not be able to mimic the exact condition of human disk herniation. Mouse was the species of choice due to the availability of FPR1$^{-/-}$ strain. Larger animals such as rabbits might be employed in the future to render better imaging resolution. Secondly, although disk puncture has been shown as a reliable model to initiate herniation and injury-associated inflammation in IVD [22–24], it is an acute injury model not reflecting a chronic process of disk herniation. Other models such as mechanical loading (compression) induced disk herniation might be adopted to delineate the episode of leukocyte infiltration from an alternative perspective [25–27].

In conclusion, for the first time, infiltration of neutrophils and macrophages was targeted and detected directly and non-invasively in a mouse disk herniation model with molecular imaging techniques. FPR1-mediated binding and specificity of peptide cFLFLF were confirmed with FPR1$^{-/-}$ mice. Imaging results were correlated with time-dependent leukocyte infiltration in disk herniation site. These findings would provide a foundation for employing FPR1-specific peptide cFLFLF as a target-specific carrier to deliver therapeutic agents via peripheral vein injection to treat discogenic low back pain.

Acknowledgments

The current study was funded by NIH grants NIAMS R21AR057512 and RO1AR064792.

References

1. Andersson GBJ. Epidemiological features of chronic low-back pain. Lancet. 1999; 354:581–585. [PubMed: 10470716]
2. Katz JN. Lumbar disc disorders and low-back pain: socioeconomic factors and consequences. J Bone Joint Surg. 2006; 88:21–24. [PubMed: 16595438]
3. Pillastrini P, Gardenghi I, Bonetti F, et al. An updated overview of clinical guidelines for chronic low back pain management in primary care. Joint Bone Spine. 2012; 79:176–185. [PubMed: 21565540]
4. Molinos M, Almeida CR, Caldeira J, et al. Inflammation in intervertebral disc degeneration and regeneration. J Royal Soc Interface. 2015; 12:20150429.
5. Risbud MV, Shapiro IM. Role of cytokines in intervertebral disc degeneration: pain and disc-content. Nat Rev Rheumatol. 2014; 10:44–56. [PubMed: 24166242]
6. Bufe B, Schumann T, Kappl R, et al. Recognition of bacterial signal peptides by mammalian formyl peptide receptors: a new mechanism for sensing pathogens. J Biol Chem. 2015; 290:7369–7387. [PubMed: 25605714]
7. Chen J, Cheng H, Dong Q, et al. [99mTc]cFLFLF for early diagnosis and therapeutic evaluation in a rat model of acute osteomyelitis. Molr imaging Biol. 2015; 17:337–344.
8. Xiao L, Zhang Y, Liu Z, et al. Synthesis of the cyanine 7 labeled neutrophil-specific agents for noninvasive near infrared fluorescence imaging. Bioorg Med Chem Lett. 2010; 20:3515–3517. [PubMed: 20488705]
9. Zhang Y, Xiao L, Chordia MD, et al. Neutrophil targeting heterobivalent SPECT imaging probe: cFLFLF-PEG-TKPPR-99mTc. Bioconj Chem. 2010; 21:1788–1793.
10. Jin L, Liu Q, Scott P, et al. Annulus fibrosus cell characteristics are a potential source of intervertebral disc pathogenesis. PLoS One. 2014; 9:e96519. [PubMed: 24796761]

11. Xiao L, Zhang Y, Berr SS, et al. A novel near-infrared fluorescence imaging probe for *in vivo* neutrophil tracking. Mol Imaging. 2012; 11:372–382. [PubMed: 22954181]
12. Ray A, Dittel BN. Isolation of mouse peritoneal cavity cells. 2010; doi: 10.3791/1488
13. Jin L, Wan Y, Shimer AL, Shen FH, Li XJ. Intervertebral disk-like biphasic scaffold—demineralized bone matrix cylinder and poly(polycaprolactone triol malate)—for interbody spine fusion. J Tissue Eng. 2012; doi: 10.1177/2041731412454420
14. Liu Q, Jin L, Shen FH, Balian G, Li XJ. Fullerol nanoparticles suppress inflammatory response and adipogenesis of vertebral bone marrow stromal cells—a potential novel treatment for intervertebral disc degeneration. Spine. 2013; J13:1571–1580.
15. Woertgen CMD, Rothoerl RDMD, Brawanski AMDP. Influence of macrophage infiltration of herniated lumbar disc tissue on outcome after lumbar disc surgery. Spine. 2000; 25:871–875. [PubMed: 10751300]
16. Doita MMD, Kanatani TMD, Harada TMD, Mizuno KMD. Immunohistologic study of the ruptured intervertebral disc of the lumbar spine. Spine. 1996; 21:235–241. [PubMed: 8720410]
17. Rothoerl RD, Woertgen C, Brawanski A. Pain resolution after lumbar disc surgery is influenced by macrophage tissue infiltration. A prospective consecutive study on 177 patients. J Clin Neurosci. 2002; 9:633–636. [PubMed: 12604272]
18. Hamamoto HMD, Miyamoto HMD, Doita MMD, et al. Capability of nondegenerated and degenerated discs in producing inflammatory agents with or without macrophage interaction. Spine. 2012; 37:161–167. [PubMed: 21494199]
19. Takada T, Nishida K, Maeno K, et al. Intervertebral disc and macrophage interaction induces mechanical hyperalgesia and cytokine production in a herniated disc model in rats. Arthritis Rheum. 2012; 64:2601–2610. [PubMed: 22392593]
20. Locke LW, Chordia MD, Zhang Y, et al. A novel neutrophil-specific PET imaging agent: cFLFLFK-PEG-64Cu. J Nucl Med. 2009; 50:790–797. [PubMed: 19372473]
21. Gao J-L, Lee EJ, Murphy PM. Impaired antibacterial host defense in mice lacking the N-formylpeptide receptor. J Exp Med. 1999; 189:657–662. [PubMed: 9989980]
22. Liang H, Ma S-Y, Feng G, Shen FH, Joshua Li X. Therapeutic effects of adenovirus-mediated growth and differentiation factor-5 in a mice disc degeneration model induced by annulus needle puncture. Spine J. 2010; 10:32–41. [PubMed: 19926342]
23. Martin JT, Gorth DJ, Beattie EE, et al. Needle puncture injury causes acute and long-term mechanical deficiency in a mouse model of intervertebral disc degeneration. J Orthop Res. 2013; 31:1276–1282. [PubMed: 23553925]
24. Michalek AJ, Buckley MR, Bonassar LJ, Cohen I, Iatridis JC. The effects of needle puncture injury on microscale shear strain in the intervertebral disc annulus fibrosus. Spine J. 2010; 10:1098–1105. [PubMed: 20971041]
25. Walter BA, Korecki CL, Purmessur D, et al. Complex loading affects intervertebral disc mechanics and biology. Osteoarth Cartilage. 2011; 19:1011–1018.
26. Yurube T, Hirata H, Kakutani K, et al. Notochordal cell disappearance and modes of apoptotic cell death in a rat tail static compression-induced disc degeneration model. Arthritis Res Ther. 2014; 16:R31. [PubMed: 24472667]
27. Ding F, Shao Z-W, Yang S-H, et al. Role of mitochondrial pathway in compression-induced apoptosis of nucleus pulposus cells. Apoptosis. 2012; 17:579–590. [PubMed: 22392483]

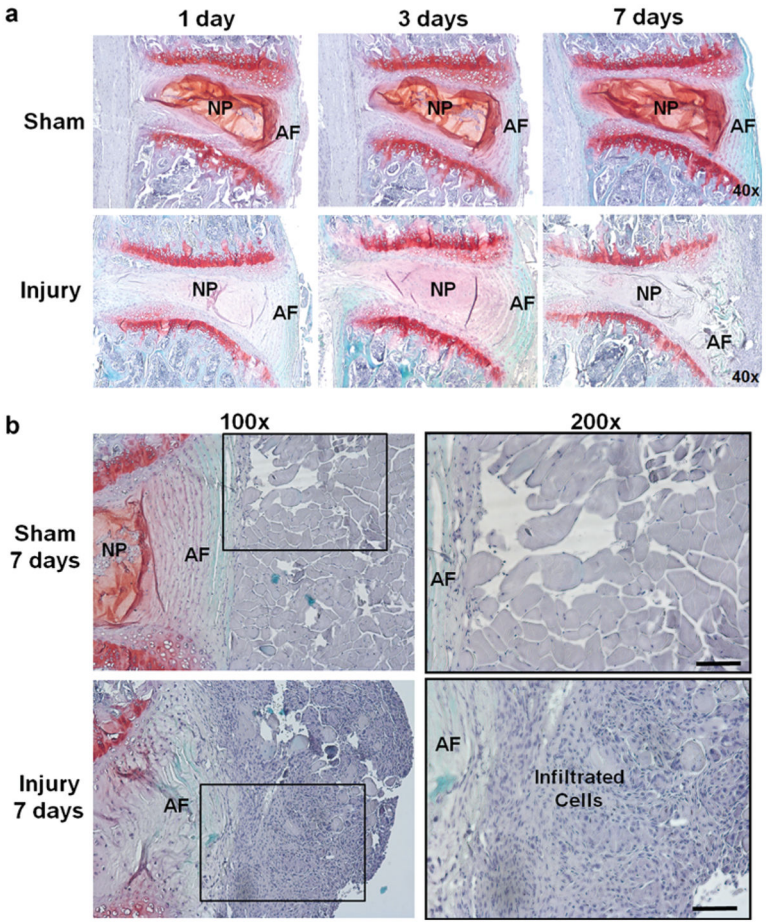

Fig. 1.

Safranin-O staining of injury and sham disks in WT mice. **a** At various time points (1, 3, and 7 days) after surgery, punctured disks demonstrated structural change and decreased proteoglycan content confirming disk herniation induced by the needle puncture (×40). **b** Higher magnification images of safranin-O staining illustrated significant amount of inflammatory cell infiltration in the region adjacent to punctured AF in injured disks at 7 days after surgery (*lower row*), whereas no such cell infiltration was found in the sham group (*upper row*). The *black square in the left column* (×100) suggested tissue area magnified in the right column (×200) (*scale bar* = 100 μm).

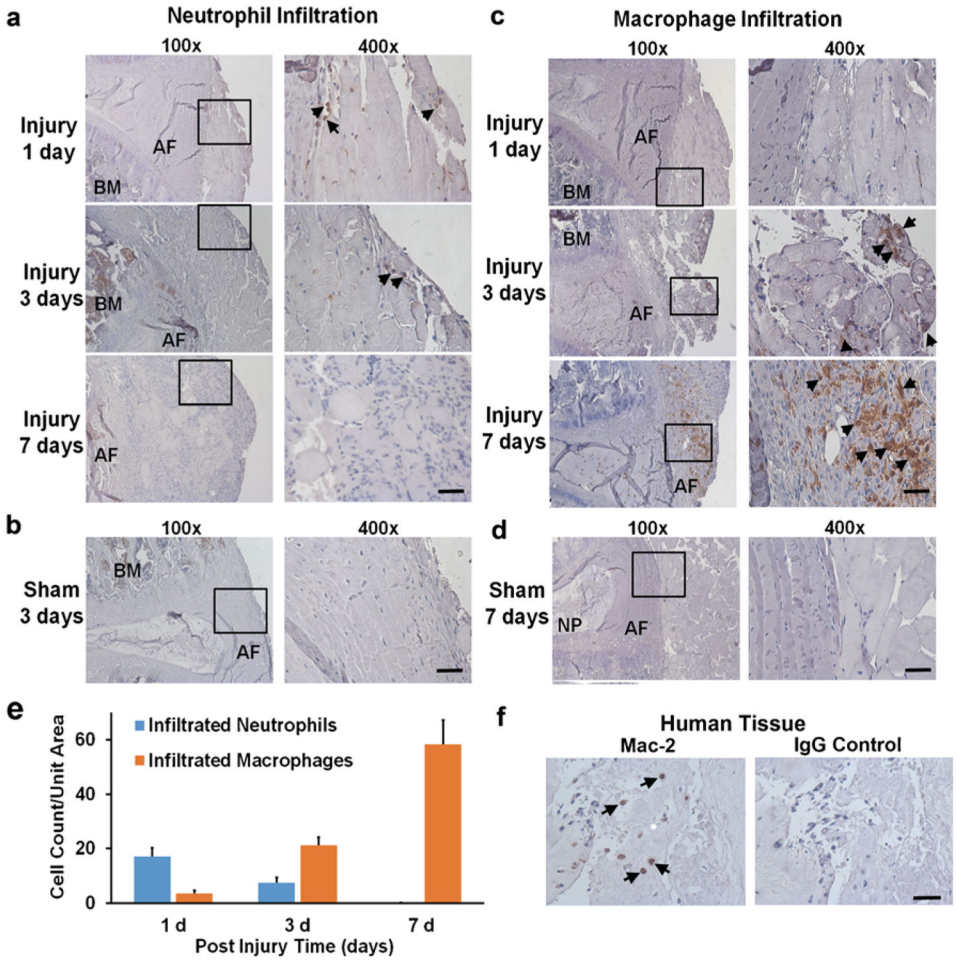

Fig. 2.

Immunohistochemical staining of neutrophils and macrophages. **a** Neutrophils started to infiltrate in the anterior region of punctured AF starting at post injury day 1 (*arrows*), remained in the same region at day 3 (*arrows*), and disappeared at day 7 in mice. **b** No neutrophil was observed in the sham mice. **c** Macrophage was not detected in the anterior region of AF at day 1 (*arrows*), however, started to appear at a mild degree at day 3 (*arrows*), and become massively present at day 7 (*arrows*) post injury in mice. **d** Few macrophages were observed up to 7 days post surgery in the sham mice. **e** Amount of infiltrated neutrophils and macrophages per unit tissue volume (0.79×10^{-3} mm^3) was plotted against various time points after mouse disk puncture. **f** Immunopositive Mac-2 staining suggested macrophage infiltration in human soft tissue surrounding severely herniated disks (*left*), while IgG control (*right*) showed no signal. Positive immunostaining cells were shown in *brown color* at ×400 (*scale bar* = 50 μm). *BM* bone marrow.

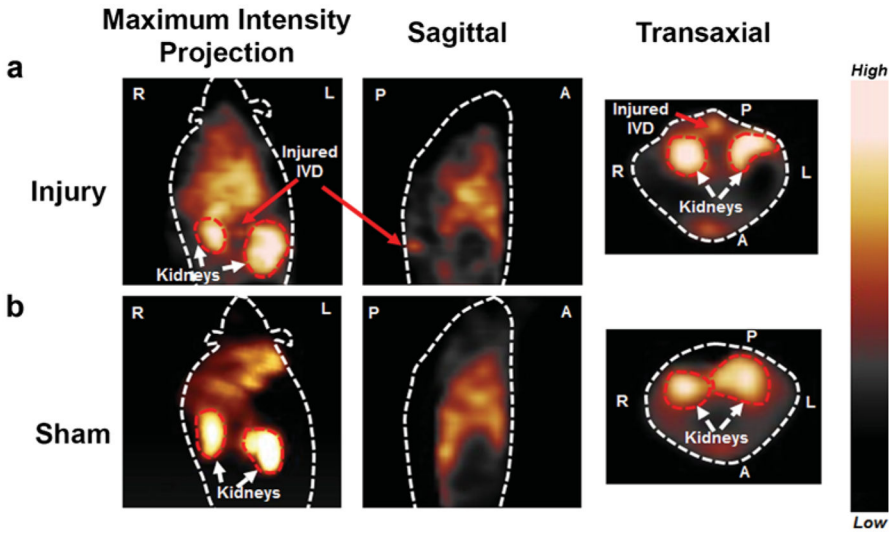

Fig. 3.

Representative SPECT imaging of [^{99m}Tc]HYNIC-PEG-cFLFLF of injury and sham mice at post surgery day 7. **a** Maximum intensity projection (MIP) at coronal view, sagittal and transverse images showed strong radioactive signal accumulation in the punctured disk area of injured mice group at 2 h post probe injection (kidneys in transaxial view served as location references) ($n = 4$). **b** In contrast, no focal signal was observed in the corresponding region of sham mice group ($n = 4$). Image orientations were labeled as left (*L*), right (*R*), anterior (*A*), and posterior (*P*).

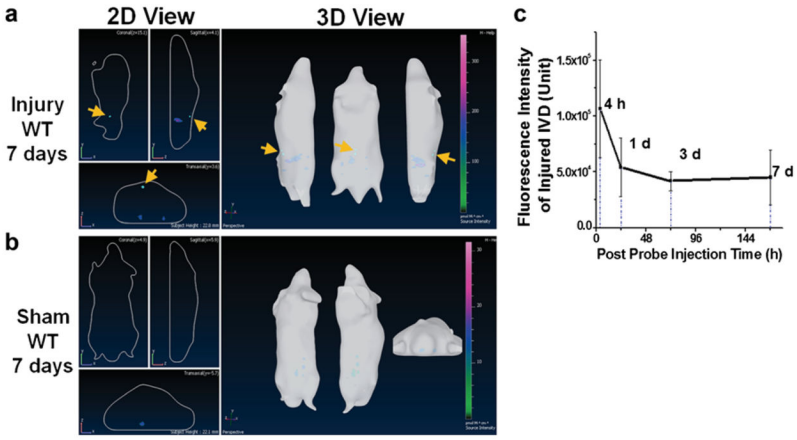

Fig. 4.

Representative *in vivo* NIRF imaging with cFLFLF-PEG-Cy7 at 7 days post probe injection. **a** Strong fluorescence signal was identified around injured disks on lumbar spines of WT mice, whereas **b** no signal was detectable in the corresponding lumbar region of sham. **c** *In vivo* observed fluorescence intensity of disk injury region was plotted against post probe injection time ($n = 5$).

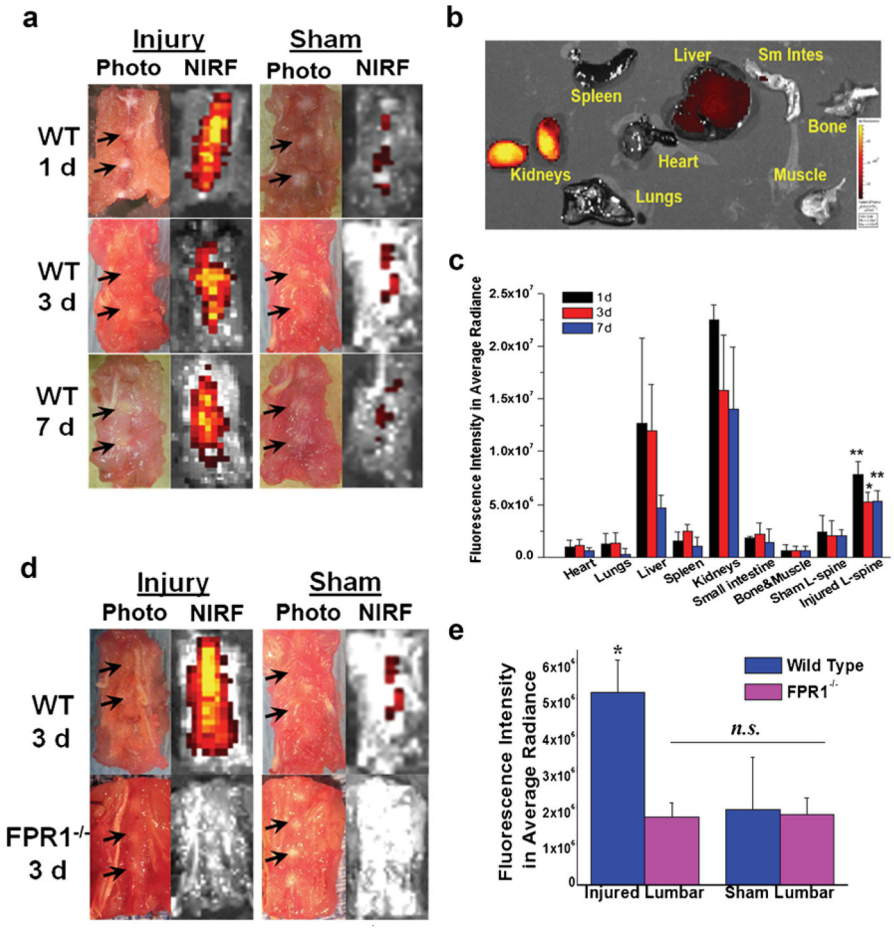

Fig. 5.

Ex vivo NIRF disk imaging of WT and FPR1$^{-/-}$ mice with cFLFLF-PEG-Cy7. **a** Representative photographs and NIRF images of WT lumbar spines containing both injured and intact disks at various time points post probe injection. **b** Organ distribution profile of cFLFLF-PEG-Cy7 at 7 days post probe injection. **c** Epi-fluorescence intensity of various organs, tissues, and punctured and sham lumbar spines at 1, 3, and 7 days post probe injection ($n = 5$ per group). *$p = 0.0084$ compared to sham lumbar at 3 days, **$p = 0.0027$ compared to sham lumbar at 1 and 7 days, respectively. **d** Representative fluorescence imaging of WT and FPR1$^{-/-}$ lumbar spine containing punctured and intact disks at 3 days post probe injection (images were displayed under the same color scale). **e** Fluorescence intensity of injury and sham lumbar for wild-type and FPR1$^{-/-}$ mice ($n = 5$ per group). For WT/injury group, *$p = 0.0084$ vs. WT/sham, *$p = 0.0035$ vs. sham/FPR$^{-/-}$, *$p = 0.0029$ vs. injury/FPR$^{-/-}$ compared to all other groups. No statistically significant difference was observed among sham/WT, injury/FPR1$^{-/-}$, and sham/FPR1$^{-/-}$ groups ($p = 0.85$ for injury/FPR1$^{-/-}$ vs. sham/FPR1$^{-/-}$, $p = 0.75$ for injury/FPR1$^{-/-}$ vs. sham/WT).

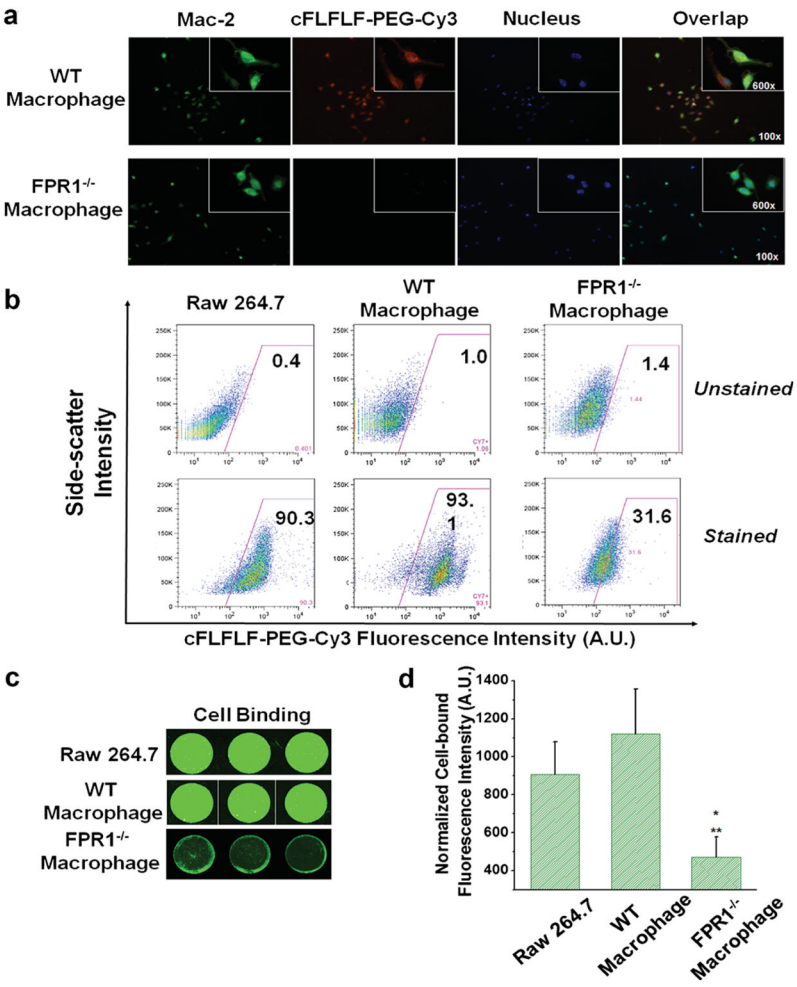

Fig. 6.

In vitro binding assays of peptide cFLFLF-PEG-Cy3 (or Cy7) with intraperitoneal harvested macrophages. **a** Immunofluorescence staining of peritoneal macrophage cells. **b** FACS exhibited predominant binding of cFLFLF-PEG-Cy3 with both RAW 264.7 and WT but not FPR1$^{-/-}$ macrophages. **c** A direct cell binding assay was performed in 96-well plates and detected by LI-COR Odyssey Infrared Imaging System, further confirming the FPR1-mediated binding specificity as seen by stronger fluorescence intensity bound to RAW 264.7 and WT macrophages than FPR1$^{-/-}$ cells. **d** Quantitative fluorescence intensities of each cell type displayed in **c** were plotted (*$p = 0.008$ for FPR1$^{-/-}$ vs. RAW cells, **$p = 0.002$ for FPR1$^{-/-}$ vs. WT cells). Note that the selection of using Cy7 or Cy3-labeled peptide was based on the preferred instrumental settings.